

Simulating the transportation and dispersal of volcanic ash cloud with initial condition created by 3D plume model

Zhixuan Cao^{1,5}, Abani Patra^{1,2}, Marcus Bursik³, E. Bruce Pitman⁴

¹Department of Mechanical and Aerospace Engineering, University at Buffalo, SUNY, New York, USA
²Computational and Data-enabled Science and Engineering, University at Buffalo, SUNY, New York,

³Department of Chemical Engineering, University of California, Berkeley, CA 94720, USA.

³Department of Geology, University at Albany, State University of New York, Albany, NY 12222.

⁴Department of Material Design and Innovation, University at Buffalo, SUNY, New York, NY, USA.

⁵ Ansys Inc., Lebanon, New Hampshire, USA

Key Points:

- The traditional way of generating initial condition for VATD simulation is based on empirical expression for the height-MER relation. Creating initial condition based on 3D plume model eliminates assumptions regarding ash particle distribution of initial ash cloud and improves prediction capability.
 - Initial particle distribution in vertical direction has more significant impact on transportation of ash clouds than horizontal distribution.
 - Ash particles are concentrated along intrusion height of umbrella cloud that is much lower than the plume top, which is just momentum overshoot.

20 **Abstract**

21 VATD (volcanic ash transportation and dispersion) models require initial conditions, which
 22 describe the initial locus of ash that is then transported. Most VATD models use a line
 23 source of some prescribed shape calibrated against an empirical expression for the height-
 24 MER relation. Such empirical vertical ash distributions may not be good representations
 25 of actual vertical ash distributions, which usually vary from case to case and have com-
 26 plex dependencies on eruption source parameters and atmospherics conditions. 3D (three-
 27 dimensional) plume models provide an alternative way to create initial ash cloud with-
 28 out any assumption regarding plume geometry. By eliminating assumed behavior asso-
 29 ciated with the semiempirical plume geometry, the predict capacity of VATD simulation
 30 would be improved. However, no VATD simulation adopts initial condition created from
 31 3D plume simulation yet. We explore this option for the first time in this paper. A vol-
 32 canic plume model based on Lagrangian method is adopted to cooperate with another
 33 Lagrangian VATD model to demonstrate implementation details. The importance of ini-
 34 tial condition is shown in sensitivity analyses which prove that volcanic ash transpor-
 35 tation simulation is much more sensitive to initial condition than all other input param-
 36 eters. Further investigation reveals that initial particle distribution in vertical direction
 37 has more significant impact on transportation of ash clouds than horizontal distribution.
 38 Comparison also indicates that ash particles are concentrated along intrusion height of
 39 umbrella cloud that is much lower than the plume top, which is just momentum over-
 40 shoot.

41 **1 Introduction**

42 **1.1 Volcanic Ash Transportation Forecast**

43 The fine-grained fraction of tephra (volcanic ash) can be widely dispersed and can
 44 lead to a degradation of air quality and pose threats to aviation. Identification of vol-
 45 canic ash helps schedule the flights accordingly to avoid flying through area where ash
 46 presents. Numerical estimation of ash distribution using known wind fields is necessary
 47 if we are to accurately predict ash cloud evolution. Numerous VATD (volcanic ash trans-
 48 portation and dispersion) models have been developed by both civil and military avi-
 49 ation or meteorological agencies to provide forecasts of ash cloud motion (Witham et al.,
 50 2007). New techniques have been integrating with VATD to satisfy increasing demands
 51 for model accuracy and forecast reliability. This paper explores an alternative way for
 52 creating initial condition for VATD simulations, which promises to improve predict ca-
 53 pability and accuracy.

54 As has been reported (e.g. Fero, Carey, & Merrill, 2009) and will be confirmed in
 55 this paper, initial condition has significant effects on simulation of volcanic ash trans-
 56 portation. Traditional VATD simulation usually requires key global descriptors of the
 57 volcanic plumes. It is a common practice to pick up the “best match” key global descrip-
 58 tors by parameter calibration (e.g. Fero, Carey, & Merrill, 2008; Fero et al., 2009; Zidikheri,
 59 Lucas, & Potts, 2017). Often, 1D plume models also serve as an alternative option to
 60 provide the key global descriptors. For example, Bursik et al. (2012) and Stefanescu et
 61 al. (2014) use bent (Bursik, 2001) to generate global descriptors. No matter how are these
 62 global descriptors obtained, they are used to define the initial condition for VATDs in
 63 forms of line source term which furnishes VATD with a spatio-temporal distribution of
 64 particles/mass along the eruption column. Vertical mass/particle distribution of line source
 65 term is calibrated against an empirical expression for the height-MER relation. The em-
 66 pirical expressions are written as functions of several parameters including key global de-
 67 scriptors. Sometimes, an extra step is adopted to spread ash particles of line source hor-
 68 zontally resulting in an initial ash cloud in 3D space. The horizontal spreading also de-
 69 pends on empirical expression. For example, PUFF spreads particle of line source uni-
 70 formly in the horizontal direction within a given radius. That is to say, both vertical dis-

tribution and horizontal distribution, if applicable, are based on empirical expressions. Considering the complexities of volcano eruption, the actual ash distribution in initial ash clouds should vary from case to case. It is difficult to have one general expression that suitable for all cases. So it is necessary to investigate alternatives ways for creating initial ash clouds without assumptions on plume geometry. This is one major motivation of this paper.

1.2 Numerical Tools

VATD models can be categorized into particle tracking type and advection-diffusion type. Among several available particle tracking models (e.g. Draxler & Hess, 1998; Damours, 1998; Searcy, Dean, & Stringer, 1998; Walko, Tremback, & Bell, 1995) and advection-diffusion models (e.g. Bonadonna & Houghton, 2005; Folch, Costa, & Macedonio, 2009; Schwaiger, Denlinger, & Mastin, 2012), we adopt a particle tracking model, PUFF (Searcy et al., 1998; Tanaka, 1991), as the VATD model. PUFF can take 3D ash clouds as initial condition, which makes it technically easier to cooperate with 3D plume models. PUFF initializes a discrete number of tracers that represent a sample of the eruption cloud, and calculates transport, turbulent dispersion, and fallout for each representative tracer. While a cylinder emanating from the summit to a specified maximum height is the standard approach to crudely model the geometry of a typical ash column. It minimally requires horizontal wind field data. The “restart feature” of PUFF makes it technically feasible to handle the difference between plume simulation and VATD simulation in terms of time scale and length scales.

Besides parameters calibration, 1D (one dimensional) plume models are also adopted to get global descriptors of volcanic plume. 1D plume models (e.g. Bursik, 2001; de'Michieli Vitturi, Neri, & Barsotti, 2015; Folch, Costa, & Macedonio, 2016; Mastin, 2007; Pouget, Bursik, Singla, & Singh, 2016; Woods, 1988) usually simplify the scenario and account for mass, momentum and energy conservation in 1D. Due to the simplification in 1D plume models, the entrainment of air is evaluated based on two coefficients: entrainment coefficient due to turbulence in the rising buoyant jet and the crosswind field. Different 1D models adopt different entrainment coefficients based on specific formulation or calibration against well-documented case studies. The feedback from plume to atmosphere is usually ignored in 1D models. While these 1D models generated well-matched results with 3D models for weak plumes, much greater variability is observed for strong plume scenarios, especially in terms of local variables (Costa et al., 2016). On the other hand, first principle based, entrainment coefficients free, 3D numerical models for volcanic plume (Cao, Patra, Bursik, Pitman, & Jones, 2018; Cerminara, Esposti Ongaro, & Berselli, 2016; Neri, Esposti Ongaro, Macedonio, & Gidaspow, 2003; Oberhuber, Herzog, Graf, & Schwanke, 1998; Y. J. Suzuki, Koyaguchi, Ogawa, & Hachisu, 2005) not only provides more accuracy prediction but also naturally create a 3D ash cloud, which can perfectly serves as initial condition for VATDs. However, to the best of author's knowledge, there is no VATD simulation taking such 3D ash clouds as initial condition yet. In this paper, we will carry out VATD simulation with initial ash cloud based on 3D plume simulation for the first time. Among these 3D plume models, we choose Plume-SPH (Cao et al., 2018) due to its easy availability to our group.

Theoretically, implementation techniques described in this paper can be applied for any combination of VATD model and 3D plume model even though our investigation is based on a specific VATD model and plume model.

1.3 Pinatubo Eruption

The 1991 eruption of Mountain Pinatubo is used as case study in this chapter. The Mountain Pinatubo erupted between June 12 and 16, 1991, after weeks of precursory activity. The climactic phase starts at June 15th 0441 UTC and ends around 1341 UTC

(R. Holasek, Self, & Woods, 1996). This climactic phase generated voluminous pyroclastic flows and sent Plinian and co-ignimbrite ash and gas columns to great altitudes (Scott et al., 1996). The evolution of the Pinatubo ash and SO_2 clouds was tracked using the visual spectrum (R. Holasek et al., 1996), the ultraviolet spectrum with a total ozone mapping spectrometer (TOMS) (Guo, Bluth, Rose, Watson, & Prata, 2004), and the infrared spectrum with a variety of sensors, including advanced very high-resolution radiometer (AVHRR) (Guo, Rose, Bluth, & Watson, 2004). There are also sufficient observational data to estimate the eruption condition for climactic phase of Pinatubo eruption (Y. Suzuki & Koyaguchi, 2009). The availability of calibrated eruption condition and extensive observational data regarding ash clouds transportation makes the Pinatubo eruption an ideal case for our research.

2 Setting up Simulations

2.1 Creating of Initial Ash Cloud

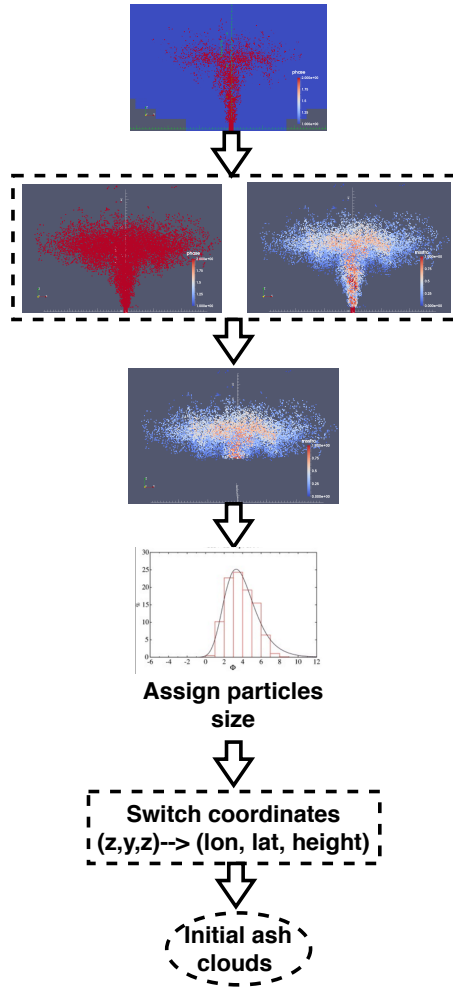
The steps to create initial ash cloud based on raw output of Plume-SPH are shown in Fig. 1. The method proposed in this paper generates initial ash cloud directly from output of 3D plume model casting aside assumptions regarding plume shape. We take Plume-SPH as an example. In case of other 3D plume models, the steps are similar. Plume-SPH is a two phases model based on a Lagrangian method, smoothed particle hydrodynamics (SPH), in which, the computational domain is discretized by SPH particles. The current version, Plume-SPH 1.0 (Cao et al., 2018), uses two types of SPH particles, particle of phase 1 to represent ambient air and particles of phase 2 to represent erupted material. Initial ash cloud is created from SPH particle of phase 2 in this paper. After reaching to the maximum height and starting spreading horizontally, particles of phase 2 forms an initial ash cloud, see, Fig. 2. 3D plume simulation is considered being completed at this point. The lower part of the plume keeps moving vertically upwards and hence is involved only minimally in horizontal ash transport. Thereby, we cut off the lower part of the plume according to an elevation threshold. Considering SPH particles are essentially discretization points and have no size, we need to assign grain size to each particle according to given distribution, mean and standard deviation of grain size (Paladio-Melosantos et al., 1996). As a consequence, the discretization points (has no size) are switch to Lagrangian tracers with sizes. The coordinates of these tracers, which are in the local Cartesian coordinate system of Plume-SPH, need to convert into PUFF's global coordinate system, which is written in terms of (*longitude, latitude, height*). PUFF then takes the initial ash clouds consisting of batch of Lagrangian tracers and propagates from time t to time $t + \Delta t$ via an advection/diffusion equation (Searcy et al., 1998).

$$\mathbf{R}_i(t + \Delta t) = \mathbf{R}_i(t) + \mathbf{W}(t)\Delta t + \mathbf{Z}(t)\Delta t + \mathbf{S}_i(t)\Delta t \quad (1)$$

Here, $\mathbf{R}_i(t)$ is the position vector of i th Lagrangian tracer at time t , \mathbf{W} accounts for wind advection, \mathbf{Z} accounts for turbulent dispersion and \mathbf{S} is the terminal gravitational fall-out velocity, which depends on tracer's size.

To summarize, it takes four steps to create initial ash cloud from raw output of Plume-SPH:

1. filtering by SPH particle type to select SPH particles that represent erupted material (phase 2)
2. filtering by an elevation threshold to cut off the plume, only leaving the upper part
3. switching discretization points to Lagrangian tracers by assigning grain size to each particle
4. converting coordinates of Lagrangian tracers into VATDs' coordinate system

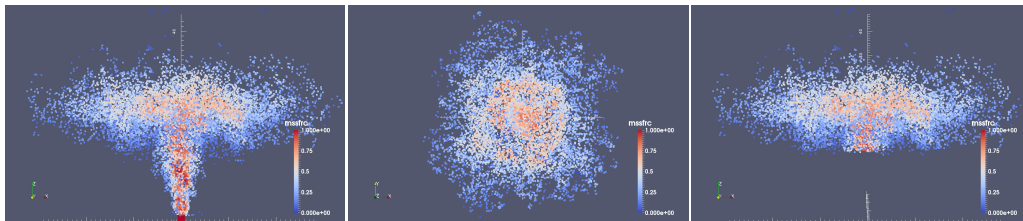


134 **Figure 1.** The work flow to create initial condition for PUFF based on raw output of Plume-
 135 SPH. Figure on the top shows raw output of Plume-SPH, where, blue particles are for phase 1
 136 (ambient air), red particles are for phase 2 (erupted material). Pictures on the second row are
 137 plume after removing SPH particles of phase 1. The left picture is colored according to mass
 138 fraction of erupted material. The figure on the third row is volcanic plume after cutting off lower
 139 portion.

196 **Table 1.** Three different methods for creating initial conditions (initial ash clouds) for PUFF
197 simulation

	No model	1D model	3D model
Maximum height	Calibration	Semiempirical	1st principle
Average height	Calibration	Conservation laws (1D)	1st principle
Vertical spread	Calibration	Semiempirical	1st principle
Column radius	Calibration	Conservation laws (1D)	1st principle
Plume shape	Semiempirical	Semiempirical	1st principle
Tracers number	Free parameter	Free Parameter	Based on simulation

174 The volcanic plume and initial ash clouds used in the case study are shown in Fig. 2.
175 It is necessary to point out that since both Plume-SPH and PUFF are based on Lagrangian
176 method, no extra step for conversion between Lagrangian particles and Eulerian grids.

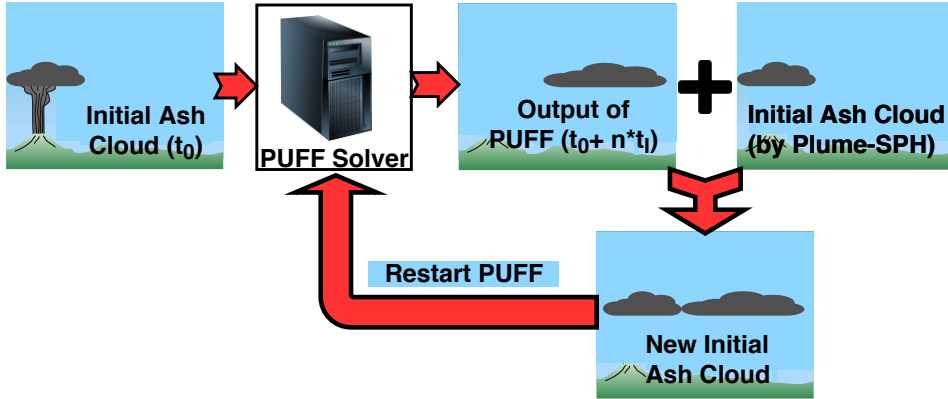


177 **Figure 2.** All particles in the pictures are of type phase 2 (phase 1 has been removed in step
178 1) at 600s after eruption, at which time, the plume has already reached the maximum height
179 and started spreading radially. Pictures from left to right are: front view of the whole plume,
180 top view of the plume and front view of the initial ash cloud, which is essentially portion of the
181 whole plume with elevation higher than a given threshold (in this picture is 15000m). Particles
182 are colored according to mass fraction of erupted material. Red represents high mass fraction
183 while blue represents low mass fraction.

184 Table 1 compares three different methods for creating initial conditions for VATD
185 simulation: 1) creating initial condition based on parameter calibration without any plume
186 model (method 1), 2) creating initial condition based on output of 1D plume model (method
187 2), 3) extracting initial ash cloud from 3D plume simulation (method 3). The first method
188 determines all global descriptors of volcanic plume based on calibration. Then create ini-
189 tial line source or ash cloud according to semiempirical plume shape expression. Both
190 other two methods depend on plume models. However 3D plume models can generate
191 initial ash cloud in 3D space while 1D plume models only obtain global descriptors of
192 plume so still need semiempirical expression to create 3D initial ash cloud. In addition,
193 the number of Lagrangian tracers is a free parameter when using semiempirical plume
194 shape expressions while it purely depends on simulation when creating initial condition
195 from 3D plume simulation results.

198 2.2 Restart PUFF

199 The plume development and ash transportation are of different time scale and length
200 scale. Spatial and temporal resolution of plume simulation is much finer than that of ash
201 transportation. The computational domain of VATD simulation is much larger than that
202 of plume simulation. It takes around tens of minutes (600s in this case) for Pinatubo plume



218 **Figure 3.** Mimic successive eruption with intermittent pulsing releasing of ash particles. t_I is
 219 the period of pulsing release. t_I equals to physical time of 3D plume simulation.

203 to reach a steady height. However the duration of eruption persists for a few hours (9
 204 hours for the climactic phase of Pinatubo eruption). It is computationally too expen-
 205 sive to do 3D plume simulation up to several hours. In order to handle the difference in
 206 time scale, we mimic successive eruption with intermittent pulsing releasing of ash par-
 207 ticles. Particularly, we restart PUFF at an interval of 600s, which is physical time of plume
 208 simulation. At every restart, we integrate the output of last PUFF simulation and the
 209 ash cloud obtained from output of Plume-SPH into a new ash cloud. This new ash cloud
 210 serves as a new initial condition when restart PUFF simulation. The interval of the puls-
 211 ing release equals to the simulation time of plume model, that is 600s in our case study.
 212 A sketch demonstrating the overall restart process is in Fig. (3). The total number of
 213 Lagrangian tracers used in PUFF equals to summation of numbers of particles in all re-
 214 leases. So the total number of tracers is not a parameter selected by user any more. Fero
 215 et al. (2008) proposed using more realistic time-dependent plume heights. We do not adopt
 216 that strategy here due to lack of well-estimated time-dependent eruption conditions, al-
 217 though the idea is straightforward to consider.

220 2.3 Sensitivity Analysis of Other Parameters

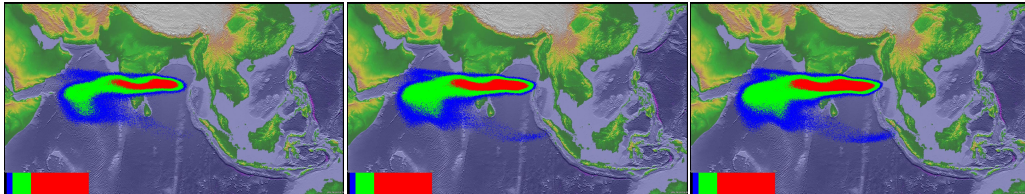
221 Besides the initial ash cloud, other input parameters for PUFF simulation are: hor-
 222 izontal diffusivity, vertical diffusivity, mean grain size, grain size standard deviation and
 223 total number of tracers. We present in this subsection systematic sensitivity studies on
 224 these parameters. We also investigate the influence of eruption duration. The sensitiv-
 225 ity analyses will serve as basis for identifying possible sources of disparities between sim-
 226 ulation and observation.

227 The sensitivity analyses illustrate that adjustment of other input parameters pro-
 228 duces negligible visual differences in VATD simulation results. Using different vertical
 229 diffusivities in range of $[100, 100000] m^2 s^{-1}$ and different horizontal diffusivities in range
 230 of $[1, 20] m^2 s^{-1}$ produces visually negligible differences. The eruption duration should
 231 depend on the actual eruption duration (or the duration of climactic phase) of a specific
 232 eruption. We conducted several simulations with eruption duration varying in range of
 233 $[5, 11] \text{hours}$ with slight different starting time of climactic phase. Table 2 lists all these
 234 simulations. However, only tiny visible differences are observed among the simulated ash
 235 transportation. The mean of grain size also has visually ignorable effects on long-term
 236 ash transportation according to our sensitivity tests varying the log mean (base 10) grain
 237 radius in a range of $[-7.3, -3.5] m$. The standard deviation, when varying in range of $[0.1, 10]$,
 238 generate ignorable difference on long-term ash transportation as well. Similar conclu-

239
 240
 241
 242
 243
 244
 245
 246
 247
 248
 249
 sion on parameter sensitivity is reported by Daniele, Lirer, Petrosino, Spinelli, and Pe-
 terson (e.g. 2009); Fero et al. (e.g. 2008). Among these parameters, the eruption dura-
 tion and beginning time shows, even though tiny, the most obvious influence on simu-
 lated ash distribution. In order to show such differences in an intuitive way, Fig. 2 shows
 simulated ash distribution corresponding to 4.9 hours duration, 9 hours duration and 11
 hours duration respectively. After 72 hours, relative to the simulation starting time, these
 three cases generate generally similar results, with high concentration ash covers almost
 the same region. The difference of lower concentration distribution is relatively more ob-
 vious. Ash cloud covers broadest area when eruption duration is 11.1 hours. To sum-
 marize, all these parameters have either tiny or ignorable affects on long-term ash dis-
 tribution simulation.

250
 251
Table 2. The starting and ending time (UT) for simulating the climactic phase of Pinatubo
 252
 eruption on June 15 1991. Observed plume height (R. Holasek et al., 1996) at different time are
 also list in the table.

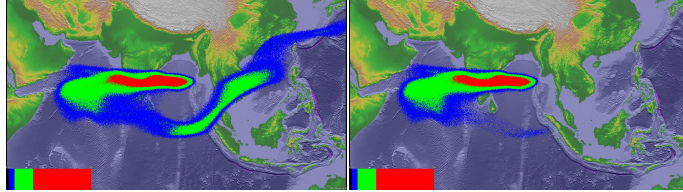
Eruption duration	4.9 hours	9 hours	10 hours	11.1 hours
Start time	0441	0441	0441	0334
Height at start time	37.5 km	37.5 km	37.5 km	24.5 km
End time	0934	1341	1441	1441
Height at end time	35 km	26.5 km	22.5	22.5 km



253
Figure 4. Simulated ash cloud distribution corresponding to eruption duration of 4.9 hours, 9
 254
 hours and 11.1 hours (from left to right) respectively. Starting and ending time for each case is in
 255
 Table 1. The contours are for ash distribution at 72 hours after eruption.

256
 257
 258
 259
 260
 261
 262
 263
 264
 265
 266
 267
 The new methodology for generating initial ash cloud introduces another new pa-
 rameter: elevation threshold. We also carry out sensitivity analysis on this parameter
 by varying the elevation threshold from 1500m (the height of the vent) to 25000m. The
 simulated ash distributions show obviously visible differences. Such influence is especially
 obvious when the elevation threshold is either very large or very small. However, vary-
 ing the elevation threshold in the range of [12000, 18000]m generates relatively small dif-
 ference in ash transportation simulation results. Figure 5 compares the simulated ash
 distribution corresponding to elevation thresholds of 1500m and 15000m. Compared with
 ash distribution for threshold of 15000m, an extra long tail appears when using eleva-
 tion threshold of 1500m. Adopting smaller elevation thresholds essentially adds more trac-
 ers at lower elevation. As the wind at different elevations are different, these newly added
 tracers at lower elevation would transpose to different directions.

272
 273
 274
 275
 The sensitivity analyses demonstrate that the initial condition for VATD simula-
 tion has the most significant effect on simulated ash distribution while all other input
 parameters have either tiny or ignorable influence. The initial ash cloud generated based
 on semiempirical expression, which is a function of several parameters, might be signif-



268 **Figure 5.** Simulated ash distribution taking initial ash clouds obtained using different el-
269 evation thresholds (1500m and 15000 m) from output of Plume-SPH. The contours are cor-
270 responding to ash concentration at 72 hours after eruption. The starting and ending time are
271 corresponding to 9 hours duration case in Table 2

276 significantly disparate from realistic ash cloud. Such initial condition might greatly compro-
277 mise the accuracy of VATDs simulation.

278 We do not carry out any investigation with respect to wind field even though it is
279 another dominant factor in VATD simulation. In the case study, we use global NOAA/OAR/ESRL
280 6-h, 2.0 reanalysis wind fields data (Compo, Whitaker, & Sardeshmukh, 2006; Compo
281 et al., 2011; Whitaker, Compo, Wei, & Hamill, 2004).

282 3 Comparison and Discussion

283 Transportation of volcanic ash resulted from Pinatubo eruption on June 15th 1991
284 is simulated using two different initial conditions. The initial condition is created in tra-
285 ditional way according to key global descriptors and semiempirical plume shape expres-
286 sion. The second initial condition is created by the new method proposed in this paper.
287 Simulated ash transportation results are compared against observation.

288 **Table 3.** List of eruption condition and material properties for plume simulation

Parameters	Units	Plume
Vent velocity	$m \cdot s^{-1}$	275
Vent gas mass fraction		0.05
Vent Temperature	K	1053
Vent height	m	1500
Mass discharge rate	$kg \cdot s^{-1}$	1.5×10^9
Specific heat of gas at constant volume	$J \cdot kg^{-1} \cdot K^{-1}$	717
Specific heat of air at constant volume	$J \cdot kg^{-1} \cdot K^{-1}$	1340
Specific heat of solid	$J \cdot kg^{-1} \cdot K^{-1}$	1100
Specific heat of gas at constant pressure	$J \cdot kg^{-1} \cdot K^{-1}$	1000
Specific heat of air at constant pressure	$J \cdot kg^{-1} \cdot K^{-1}$	1810
Density of air at vent height	$kg \cdot m^{-3}$	1.104
Pressure at vent height	Pa	84363.4

289 To create initial condition using the new method described in this paper, the plume
290 raising up process is simulated first by Plume-SPH. The eruption parameters, material
291 properties and atmosphere for the strong plume no wind case in a comparison study on
292 eruptive column models (Costa et al., 2016) are adopted. Eruption conditions and ma-
293 terial properties are listed in Table 3. Note that the density of erupted material at the
294 vent and radius of the vent can be computed from the given parameters. The eruption
295 pressure is assumed to be the same as pressure of ambient at the vent and hence is not

given in the table. The vertical profiles of atmospheric properties were obtained based on the reanalysis data from ECMWF (European Centre for Medium-Range Weather Forecasts) for the period corresponding to the climactic phase of the Pinatubo eruption. The initial ash cloud is obtained by processing the raw output of Plume-SPH following steps described in Sec. 2.

Another set of initial condition is created based on observed top height (40km) and several other parameters assigned semiempirically (Bursik et al., 2012). These parameters, namely, the global descriptors of volcanic plume, are used as parameters of semiempirical expression to get ash cloud in 3D space. See details in Table 4. The simulation parameters that control VATD simulation are the same for both simulations. As has been shown in sensitivity analyses section, these parameters have less influence on simulation results than initial condition.

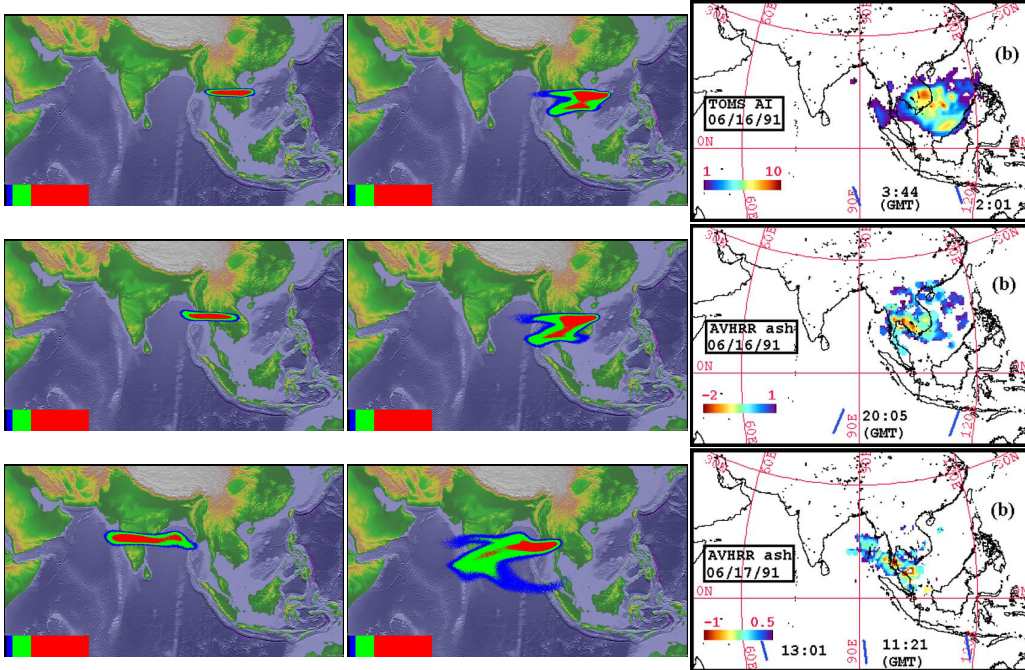
Table 4. Parameters used in VATD simulation of the climactic phase of Pinatubo eruption on June 15 1991. The first six parameters are used by semiempirical expression to create initial ash cloud. When create initial condition based on Plume-SPH model, these parameters are extracted from output of Plume-SPH model.

Parameters	Unit	Semiempirical	Plume-SPH
Maximum Height (H_{max})	m	40000	41800
Horizontal Spread (R_{max})	km	103.808	-
Vertical Spread (H_{width})	km	6.662	-
Plume Shape	-	Poisson	-
Total Ash Particles	-	1768500	1768500
Elevation Threshold	m	-	15000
Horizontal Diffusivity	m^2/s	10000	10000
Vertical Diffusivity	m^2/s	10	10
Grain Size Distribution	-	Gaussian	Gaussian
Mean of Grain Size (Radius)	mm	3.5×10^{-2}	3.5×10^{-2}
Standard Deviation of Grain Size	-	1.0	1.0
Start Time	UT	0441	0441
End time	UT	1341	1341
Simulation Duration	hour	72	72

3.1 “Plume-SPH + PUFF” and “Semiempirical Initial Cloud + PUFF”

The simulation results using different initial conditions are compared with TOMS images and AVHRR BTD ash cloud map in Fig. 6.

The differences between simulated ash transportation by “Semiempirical initial cloud +PUFF” and “Plume-SPH+PUFF” are obvious. The simulated ash concentration based on initial condition created from Plume-SPH is much closer to observation than that based on semiempirical plume shape expression. Around 23 hours and 31 hours after the beginning of the climactic phase, “Plume-SPH + PUFF” simulation generates ash images that generally close to observational image, especially the location where high concentration ash presents. However, these ash at near west to Pinatubo mountain observed in satellite images does not show up in “Plume-SPH + PUFF” simulation results. This disparity is very possible due to the fact that the Mountain Pinatubo continued erupting after climactic phase while our simulation only simulates the climactic phase. The ash released after climactic phase is not accounted in our simulation results. The “Semiempirical initial cloud + PUFF” simulation, however, forecasts an ash distribution faster



315 **Figure 6.** Comparison between “Semiempirical initial cloud + PUFF” and “Plume-SPH
316 + PUFF”. Pictures from left to right are: PUFF simulation based on initial condition created
317 according to semiempirical plume shape expression, PUFF simulation based on initial condi-
318 tion generated by Plume-SPH, TOMS or AVHRR image of Pinatubo ash cloud. Ash clouds at
319 different hours after eruption are on different rows. From top to bottom, the images are corre-
320 sponding to around 23 hours after eruption (UT 199106160341), 31 hours after eruption (UT
321 199106161141), 55 hours after eruption (UT 199106171141). The observation data on the first
322 row are TOMS ash and ice map. The observation data on the second and third row are AVHRR
323 BTD ash cloud map with atmospheric correction method applied (Guo, Rose, et al., 2004).

336 and narrower than observation. The location, where the high concentration ash presents,
337 locates to the far northwest of observed ash. Around 55 hours after the beginning of the
338 climactic phase, the disparity between observation and simulation becomes more obvi-
339 ous. Ash distribution of “Semiempirical initial cloud + PUFF” simulation locates far
340 west to the observed ash. The high concentration area of “Plume-SPH + PUFF” sim-
341 ulation, even though closer to observation than that of “Semiempirical initial cloud +PUFF”,
342 is still faster than observation.

343 At the stage of ash transportation simulation, except for the initial condition, both
344 simulations adopt the same parameters and wind field data. That is to say, the only dif-
345 ference between these two simulations is the initial condition. Recall the initial condi-
346 tion has most significant influence on ash transportation simulation. It is very possible
347 that the big difference between simulation results by “Plume-SPH+PUFF” and “Semiem-
348 pirical initial cloud +PUFF” is attribute to the initial condition.

349 3.2 Discussion Regarding Maximum Height (H_{max})

350 In this section, we majorly focus on the vertical distribution of ash particles in ini-
351 tial ash cloud. The majority of volcanic ash particles usually present a lower elevation
352 than maximum height. For instance, R. Holasek et al. (1996); R. E. Holasek, Woods, and
353 Self (1996) reported the maximum Pinatubo plume height as high as around 39km while

the cloud heights were estimated at $20 \sim 25\text{km}$, Self, Zhao, Holasek, Torres, and King (1996) report the maximum plume height could be $> 35\text{km}$ and the plume heights are $23 \sim 28\text{km}$ after $15 \sim 16$ hours. The neutral buoyant regions of the Pinatubo aerosol estimated by different measurements are: $17 \sim 26\text{km}$ (lidar) by DeFoor, Robinson, and Ryan (1992), $20 \sim 23\text{km}$ (balloon) by Deshler, Hofmann, Johnson, and Rozier (1992), $17 \sim 28\text{km}$ (lidar) by Jäger (1992), and $17 \sim 25\text{km}$ (lidar) by Avdyushin et al. (1993). Based on comparison between simulated cloud with early infrared satellite images of Pinatubo, Fero et al. (2008) reported that the majority of ash was transported between 16km and 18km . This is physically understandable as particles are concentrated along intrusion height of umbrella cloud, not near top because the plume top is due to momentum overshoot. However, the empirical expressions for the height-MER relation, which are commonly adopted to create initial conditions for VATD simulation, tends to place majority of ash particles closer to top if use observed maximum height in the empirical expressions.

Here we check two commonly used plume shapes, the Poisson and Suzuki. For Poisson plume shape, the vertical height of ash particles are determined according to Eq. (2).

$$H = H_{max} - 0.5H_{width} * P + H_{width}R \quad (2)$$

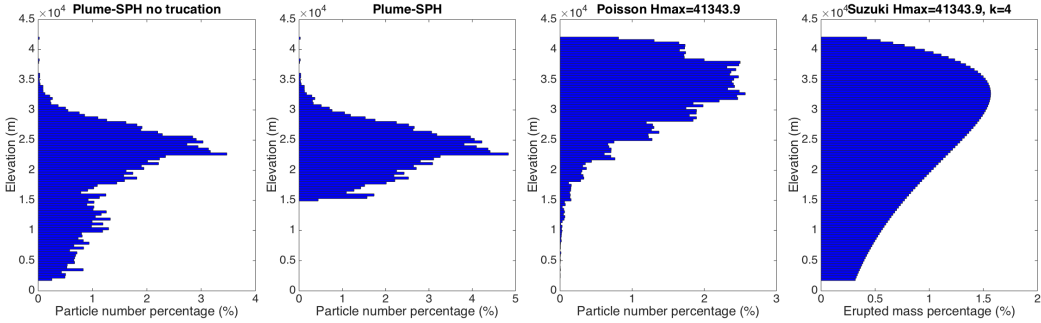
where P is an integral value drawn from a Poisson distribution of unit mean, R is a uniformly distributed random number between 0 and 1, H_{max} is the maximum plume height, H_{width} represents an approximate vertical range over which the ash will be distributed. For Suzuki plume shape (T. Suzuki et al., 1983), volcano ash mass vertical distribution is assumed to follow the Suzuki equation (Eq. (3)).

$$Q(z) = Q_m * \frac{k^2(1 - z/H_{max})\exp(k(z/H_{max} - 1))}{H_{max}[1 - (1 + k)\exp(-k)]} \quad (3)$$

Where Q_m is the total mass of erupted material, k is shape factor, which is an adjustable constant that controls ash distribution with height. A low value of k gives a roughly uniform distribution of mass with elevation, while high values of k concentrate mass near the plume top.

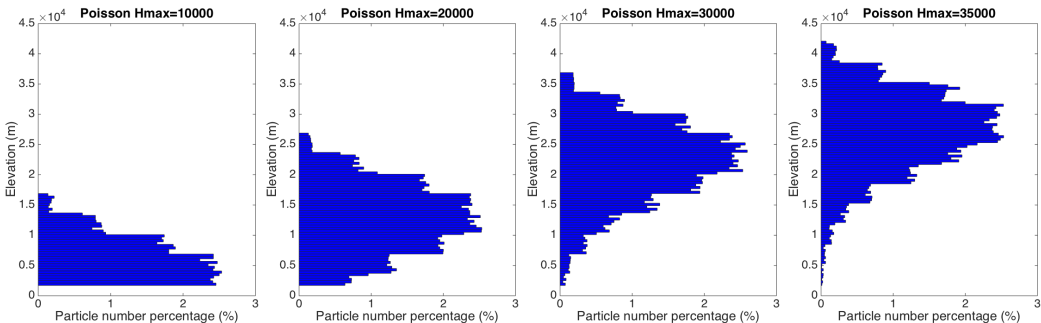
Particle distribution (in terms of mass percentage or particle number percentage) in vertical direction in the initial ash cloud are shown in Fig. 7. In that figure, the vertical particle distribution based on Plume-SPH output is compared with vertical particle distribution created based on semiempirical shape expressions. Both Poisson and Suzuki distribution in Fig. 7 take $H_{max} = 40000\text{m}$, which is close to reported observation of maximum height. When adopting Poisson plume shape, the majority of the particles are between $30\text{km} \sim 40\text{km}$. Obviously, Poisson distributes majority ash at a much higher elevation than observations (e.g. Fero et al., 2008). As for Suzuki, the majority of ash particles also distribute in a range that significantly higher than 25km . As for initial ash cloud based on Plume-SPH simulation, the major population of ash particles distribute between $17\text{km} \sim 28\text{km}$, which match well with observations. The maximum height is also consistent with observation. To summarize, using semiempirical plume shape expression generates unrealistic initial ash cloud even if we use observed plume maximum height.

For Poisson and Suzuki plume shape, vertical distribution of ash particles can't be lower down without changing the maximum height. To distribute major population of ash particles at lower elevation, the maximum height has to be reduced to a value smaller than observed maximum height. Adjusting parameters such as maximum height in the emperical expression is actually the traditional source term calibration method. A set of initial ash clouds using different maximum heights based on Poisson plume shape is shown in Fig. 8). The maximum heights adopted in plume shape expressions are, by no means, obtained from any plume model or observation. Except for maximum height, all other parameters for creating initial ash cloud are the same as these in Table 4. The range,



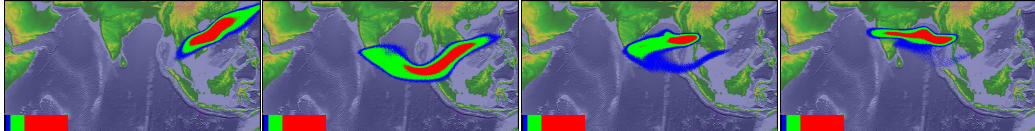
393 **Figure 7.** Particle distribution of initial ash cloud in vertical direction. The picture to the
 394 left is corresponding to initial ash cloud obtained from Plume-SPH output. The second picture
 395 is corresponding to ash distribution truncated by a elevation threshold of 15000m. The third
 396 picture is for vertical ash distribution based on Poisson distribution with maximum height equals
 397 to 40000m. Another parameter, the vertical spread, in the expression of Poisson plume shape is
 398 6662m. The picture to the right is corresponding to Suzuki distribution with maximum height
 399 equals to 40000m. Another parameter in Suzuki distribution, the shape factor, is 4. The x axis is
 400 the percentage of particle number for Plume-SPH and Poisson. For Suzuki the x axis is the mass
 401 percentage of erupted material.

411 between which major populations of ash particles locate, is lower when using smaller max-
 412 imum heights. These ash clouds created by Poisson distribution with different maximum
 413 heights are then used as initial condition in PUFF simulation, whose results are show
 414 in Fig. 9.



415 **Figure 8.** Initial particle distribution in vertical direction based on Poisson plume shape with
 416 different maximum heights. Pictures from left to right are corresponding to maximum height of
 417 10000m, 20000m, 30000m, 35000m. Another parameter, the vertical spread, in the expression of
 418 Poisson plume shape is 6662m for all cases. The x axis is the percentage of particle number. See
 419 Fig. 7 for vertical ash distribution of Plume-SPH output.

425 Figure 9 shows that the maximum height has significant influence on ash transporta-
 426 tion simulation. When the maximum height is 10000m the high concentration area is
 427 lag behind observation. While the designated maximum height is 35000m, the high con-
 428 centration area is a little bit faster and much narrower than observation. When using
 429 maximum height of 41343.9m, the high concentration area is faster and narrower than
 430 both observation and “Pume-SPH+PUFF” simulation results (see Fig. 6). The simu-
 431 lated high concentration area is closest to “Pume-SPH+PUFF” simulation results when



420 **Figure 9.** Ash transportation simulated by PUFF using different initial ash cloud created
 421 according to Poisson distribution with different maximum heights. Pictures from left to right are
 422 corresponding to maximum plume heights of 10000m, 20000m, 30000m and 35000m. All images
 423 are for simulated ash transportation around 55 hours after eruption (UT 199106171141). See the
 424 observed cloud image in Fig. 6.

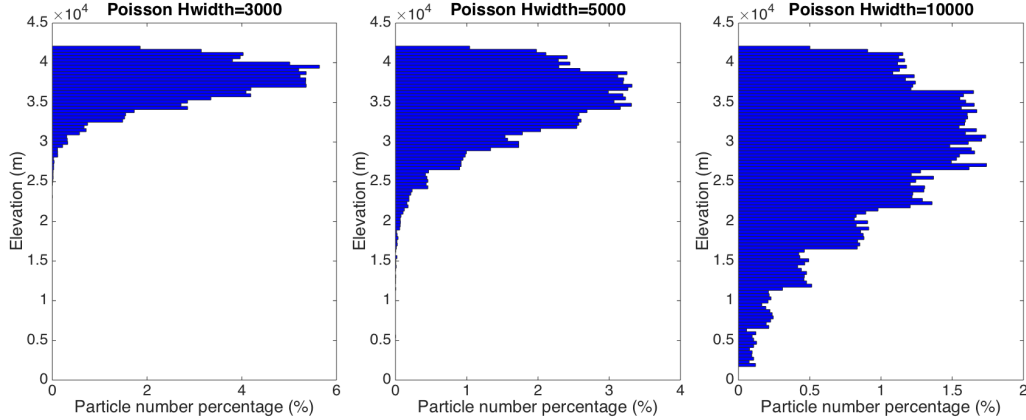
432 assigning a maximum height of 30000m. The front of volcano ash, with lower concen-
 433 tration is faster than observation locating far west to high concentration area. A lower
 434 concentration tailing area also appears in the simulation results while there is no such
 435 tail in observed image. PUFF simulation result based on calibrated maximum height of
 436 30000m shows similar footprint to, even though smaller in terms of covered area than,
 437 those of "Pume-SPH+PUFF" simulation. However, the initial ash cloud created by Pois-
 438 son distribution with maximum height around 20000m generates best match ash distri-
 439 bution with observation. That is to say, a maximum height lower than real maximum
 440 height is required by Poisson plume shape to distribute ash particles at the same eleva-
 441 tion as real ash distribution. This is physically understandable as maximum plume heights
 442 are reached due to overshoot. Our hypothesis regarding the sources of disparity between
 443 "Semiempirical initial cloud +PUFF" simulation and observation is confirmed. Since the
 444 initial condition has so dominant effect on VATD simulation, it is very necessary to ex-
 445 plore more accurate and adaptive ways for establishing the initial conditions.

446 3.3 Discussion Regarding Vertical Spread (H_{width})

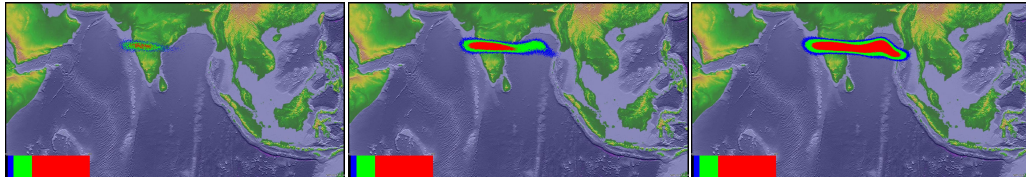
447 In previous section, the maximum height is adjusted to change vertical ash distri-
 448 bution along the source line. This section investigates another parameter in semiempir-
 449 ical poisson expression. We vary the "vertical spread" (H_{width}) in range 3km/ 10km.
 450 A set of initial ash clouds created according to different "vertical spread" is shown in Fig.
 451 10. Except for "vertical spread", all other parameters for creating initial ash cloud are
 452 the same as these in Table 4. Width of the range within which major populations of ash
 453 particles locate become narrower when a smaller value for vertical spread is used. But
 454 changing H_{width} has no obvious affect on the height at which majority of ash particles
 455 distribute. These ash clouds based on different vertical spread are then used as initial
 456 condition in PUFF simulation, whose results are show in Fig. 11.

457 Adjusting of the vertical spread can change particle distribution in vertical direc-
 458 tion and not surprisingly affect VATD simulation results. Unluckily, none of these VATD
 459 simulations based on initial ash cloud with vertical spread equals to 3km, 5km, and 10km
 460 get better results than VATD simulation based on initial condition created by a 3D plume
 461 simulation using Plume-SPH (see Fig. 11).

472 The calibrations carried out here are definitely not exhaustive. One might do more
 473 comprehensive calibration throughout the multi-dimensional (two dimensional for Pois-
 474 son distribution) parameter space and get better matched ash transportation results. With
 475 more complicated plume shape expression, one could have more control over plume shape
 476 and might be able to get initial condition that much closer to actual initial ash cloud,
 477 hence obtain more accurate ash transportation prediction. But more complicated plume
 478 shape expression usually leads to higher dimensional parameter space which requires more
 479 effort to do calibration. Even though, the degree of freedom to adjust plume shape is still
 480 limited. The new method for creating initial conditions based on 3D plume simulation



462 **Figure 10.** Vertical particle distribution based on Poisson plume shape with different “vertical
463 spread”. Pictures from left to right are corresponding to vertical spread of 3km, 5km and
464 10km. The maximum height in the expression of Poisson plume shape is 40000m for all cases.
465 The x axis is the percentage of particle number. See Fig. 7 for vertical ash distribution of Plume-
466 SPH output.



467 **Figure 11.** Ash transportation simulated by PUFF using different initial ash cloud created
468 with different vertical spread. Pictures from left to right are: PUFF simulation results based on
469 initial ash clouds with vertical spread equals to 3000mm, 5000mm and 10000m. The images are
470 corresponding to around 55 hours after eruption (UT 199106171141). See the observed cloud
471 image in Fig. 6. The simulated ash field does not adequately cover the observed ash field.

481 is more adaptive to various cases and obviates semiempirical expressions regarding plume
482 shape.

483 3.4 Horizontal Ash Distribution

484 The differences between assumed plume particle distribution and actual (or sim-
485 ulated by 3D plume) model are not only in vertical direction. How cloud horizontal par-
486 ticle distribution of the initial ash cloud affect ash transportation is investigated in this
487 section. PUFF uses a uniformly distributed random process to determine the ash par-
488 ticle location in a circle centered on the volcano site. The maximum radius (at top) is
489 given as “horizontal spread” in Table 4. The horizontal displacement from a vertical line
490 above the volcano is a random value within a circle of radius, which equals to “horizon-
491 tal spread” multiplied by the ratio of the particle height H to maximum H_{max} . So the
492 net shape of the plume is an inverted cone where particles are located directly over the
493 volcano at the lowest level and extend out further horizontally with increasing plume height.
494 As for output of Plume-SPH, an effective radius is determined according to a given thresh-
495 old of ash concentration following Cerminara, Esposti Ongaro, and Neri (2016). A time
496 averaging and spatial integration of the dynamic 3D flow fields are conducted to get rid
497 of significant fluctuations in time and space. Fig. 12 compares radius of initial ash clouds
498 created by 3D plume simulation and assumed plume shape expression adopted in PUFF.

Obviously, there is no chance for these two radius to be similar. Adjusting the parameter “horizontal spread” could not make the assumed plume shape to be similar to ash cloud created by Plume-SPH. That is to say, merely parameter calibration is not enough for such situation. It would require higher order semiempirical expression that takes more parameters.

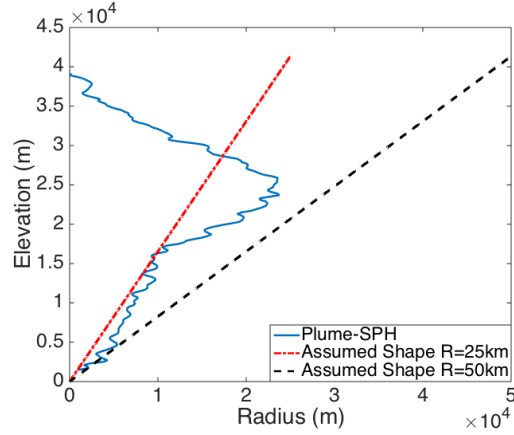


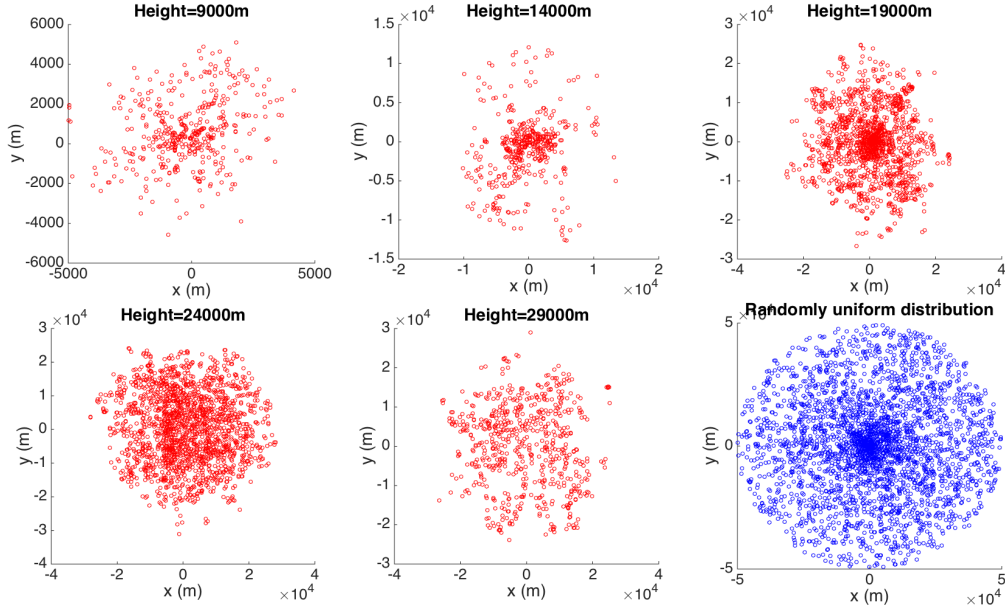
Figure 12. Comparison between radius of initial ash clouds created by 3D plume model (Plume-SPH) and assumed initial ash cloud shape in PUFF. The plume shape expression used in PUFF defines an inverted cone whose actual shape changes when “horizontal spread” takes different values. $R = 25\text{km}$ is corresponding to “horizontal spread” equals to 50km . $R = 50\text{km}$ is corresponding to “horizontal spread” equals to 100km

Comparison between cross-sectional views of the initial ash clouds is shown in Fig. 13. The cross-sectional view of assumed plume shape (last figure in Fig. 13) is similar to cross-sectional view of simulated 3D plume in general sense. However, for simulated 3D plume, the ash particle distribution on cross section varies along with height. It is hard for semiempirical expressions have such feature. In PUFF, particle distribution on cross sections is assumed to be the same.

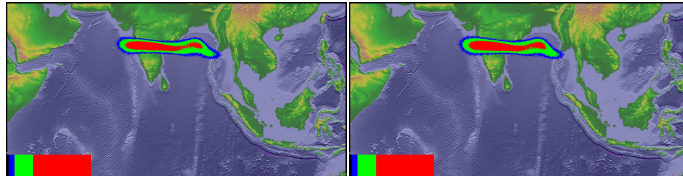
Assigning different values to “horizontal spread” has ignorable effect on VATD simulation results. We use numbers between 50km to 1600km as “horizontal spread” to create initial ash cloud for VATD, all of them generate very similar results. Figure ?? shows two different simulation results based on initial ash cloud with “horizontal spread” equals to 50km and 600km respectively. No visible differences can be told between them. This implies that horizontal distribution has less significant influence on VATD simulation results than vertical distribution.

4 Conclusion

This paper presented, for the first time, VATD simulation using intial condition created by a 3D plume model while traditional VATD simulation using initial condition created according to semiemperical plume shape expression. Case study of Pinatubo eruption demonstrates that 3D plume model can create more realistic initial ash cloud and improve accuracy of ash transportation forecast. In order to explain why we got much closer ash dispersal forecast merely by adopting alternative initial conditions, more investigations were conducted. Sensitivity analyses illustrate that initial condition has more significant effects on volcanic ash transportation forecast than most of the other parameters. Comparison of vertical ash distribution between 3D plume model, semiempirical expression and observations reveals that major population of ash particles are at much



515 **Figure 13.** Horizontal distribution of ash particles (tracers) on a cross section of initial ash
 516 cloud. PUFF assumes randomly uniform distribution of ash particle within a circle, as shown
 517 by red dots in the last figure. All other figures show ash particle distribution of initial ash cloud
 518 created by Plume-SPH at different elevations.



526 **Figure 14.** Ash transportation simulated by PUFF at around 55 hours after eruption (UT
 527 199106171141). Different values for “horizontal spread” are used to create initial ash cloud. Pic-
 528 tures to the left is corresponding to “horizontal spread” equals to 50kmm. Pictures to the right is
 529 corresponding to “horizontal spread” equals to 600kmm. The observed cloud image is in Fig. 6.

541 lower elevation than maximum height. For the case study of Pinatubo eruption, “well-
 542 matched” simulation results are observed when using maximum height of around 30km,
 543 which is much lower than observed maximum height of 40km. Calibrating of the max-
 544 imum height, vertical spread and horizontal spread shows that ash particle distribution
 545 in vertical direction has more dominant effect on VATD simulation.

546 This new method provides an alternative option for creating initial conditions for
 547 VATD simulation. Except for the disadvantage of high computational cost it helps over-
 548 come several shortcomings of existing methods. As numerical models based on first prin-
 549 ciple, 3D plume models eliminate parameterization and hence user intervention associ-
 550 ated with entrainment coefficients, thereby, improve forecast capacity of ash transpor-
 551 tation simulation. More importantly, no assumption about plume shape is needed in this
 552 new method. The plume shape generated directly by 3D simulation is more adaptive to
 553 various scenarios, thereby, could be more realistic. Contrastingly, semiempirical plume
 554 shape expressions only have several parameters to control the vertical ash particle dis-
 555 tribution of line source or the shape of initial ash cloud, it might have difficulties to gen-
 556 erate initial condition that close to reality for some eruptions. In theory, the method-

557 ology can be applied to any combination of VATD model and 3D plume model even though
 558 a specific 3D plume model and VATD model is used in this paper.

559 The full range of research issues raised by the numerical forecasting of volcanic clouds
 560 is many and diverse. We described in this paper the effect of initial conditions on nu-
 561 matical forecasts of volcanic ash transportation simulation. Wind field, another impor-
 562 tant factor in volcanic ash transportation simulation is not discussed in the present work.
 563 Some other aspects, such as small scale physical processes, even though plays less roles,
 564 might need to be included by VATDs to improve accuracy for particular eruption event.
 565 In addition, the eruption condition, hence the initial ash clouds, are subject to change
 566 during eruption even during climactic phase of eruption. More realistic, time-dependent,
 567 initial condition for VATDs can be created from 3D plume simulation with time-dependent
 568 eruption conditions.

569 Acknowledgments

570 Support for the Twentieth Century Reanalysis Project dataset is provided by the U.S.
 571 Department of Energy, Office of Science Innovative and Novel Computational Impact
 572 on Theory and Experiment (DOE INCITE) program, and Office of Biological and En-
 573 vironmental Research (BER), and by the National Oceanic and Atmospheric Adminis-
 574 tration Climate Program Office.

575 References

- 576 Avdyushin, S., Tulinov, G., Ivanov, M., Kuzmenko, B., Mezhuev, I., Nardi, B., ...
 577 Chanin, M.-L. (1993). 1. spatial and temporal evolution of the optical thick-
 578 ness of the pinatubo aerosol cloud in the northern hemisphere from a network
 579 of ship-borne and stationary lidars. *Geophysical research letters*, 20(18), 1963–
 580 1966.
- 581 Bonadonna, C., & Houghton, B. (2005). Total grain-size distribution and volume of
 582 tephra-fall deposits. *Bulletin of Volcanology*, 67(5), 441–456.
- 583 Bursik, M. (2001). Effect of wind on the rise height of volcanic plumes. *Geophys.*
 584 *Res. Lett*, 28(18), 3621–3624.
- 585 Bursik, M., Jones, M., Carn, S., Dean, K., Patra, A., Pavolonis, M., ... others
 586 (2012). Estimation and propagation of volcanic source parameter uncertainty
 587 in an ash transport and dispersal model: application to the eyjafjallajokull
 588 plume of 14–16 april 2010. *Bulletin of volcanology*, 74(10), 2321–2338.
- 589 Cao, Z., Patra, A., Bursik, M., Pitman, E. B., & Jones, M. (2018). Plume-sph 1.0: a
 590 three-dimensional, dusty-gas volcanic plume model based on smoothed particle
 591 hydrodynamics. *Geoscientific Model Development*, 11(7), 2691–2715.
- 592 Cerminara, M., Esposti Ongaro, T., & Berselli, L. (2016). Ashee-1.0: a compressible,
 593 equilibrium-eulerian model for volcanic ash plumes. *Geoscientific Model Devel-*
 594 *opment*, 9(2), 697–730.
- 595 Cerminara, M., Esposti Ongaro, T., & Neri, A. (2016). Large eddy simulation
 596 of gas-particle kinematic decoupling and turbulent entrainment in volcanic
 597 plumes. *Journal of Volcanology and Geothermal Research*.
- 598 Compo, G. P., Whitaker, J. S., & Sardeshmukh, P. D. (2006). Feasibility of a 100-
 599 year reanalysis using only surface pressure data. *Bulletin of the American Me-*
 600 *teorological Society*, 87(2), 175–190.
- 601 Compo, G. P., Whitaker, J. S., Sardeshmukh, P. D., Matsui, N., Allan, R. J., Yin,
 602 X., ... others (2011). The twentieth century reanalysis project. *Quarterly*
 603 *Journal of the Royal Meteorological Society*, 137(654), 1–28.
- 604 Costa, A., Suzuki, Y., Cerminara, M., Devenish, B., Esposti Ongaro, T., Herzog,
 605 M., ... others (2016). Results of the eruptive column model inter-comparison
 606 study. *Journal of Volcanology and Geothermal Research*.
- 607 Daniele, P., Lirer, L., Petrosino, P., Spinelli, N., & Peterson, R. (2009). Applica-

- tions of the puff model to forecasts of volcanic clouds dispersal from etna and vesuvio. *Computers & Geosciences*, 35(5), 1035–1049.
- DeFoor, T. E., Robinson, E., & Ryan, S. (1992). Early lidar observations of the june 1991 pinatubo eruption plume at mauna loa observatory, hawaii. *Geophysical research letters*, 19(2), 187–190.
- Degruyter, W., & Bonadonna, C. (2012). Improving on mass flow rate estimates of volcanic eruptions. *Geophysical Research Letters*, 39(16).
- de'Michieli Vitturi, M., Neri, A., & Barsotti, S. (2015). Plume-mom 1.0: A new integral model of volcanic plumes based on the method of moments. *Geoscientific Model Development*, 8(8), 2447–2463.
- Deshler, T., Hofmann, D., Johnson, B., & Rozier, W. (1992). Balloonborne measurements of the pinatubo aerosol size distribution and volatility at laramie, wyoming during the summer of 1991. *Geophysical research letters*, 19(2), 199–202.
- Devenish, B. (2013). Using simple plume models to refine the source mass flux of volcanic eruptions according to atmospheric conditions. *Journal of Volcanology and Geothermal Research*, 256, 118–127.
- Draxler, R. R., & Hess, G. (1998). An overview of the hysplit_4 modelling system for trajectories. *Australian meteorological magazine*, 47(4), 295–308.
- Damours, R. (1998). Modeling the etex plume dispersion with the canadian emergency response model. *Atmospheric Environment*, 32(24), 4335–4341.
- Fero, J., Carey, S. N., & Merrill, J. T. (2008). Simulation of the 1980 eruption of mount st. helens using the ash-tracking model puff. *Journal of Volcanology and Geothermal Research*, 175(3), 355–366.
- Fero, J., Carey, S. N., & Merrill, J. T. (2009). Simulating the dispersal of tephra from the 1991 pinatubo eruption: implications for the formation of widespread ash layers. *Journal of Volcanology and Geothermal Research*, 186(1), 120–131.
- Folch, A., Costa, A., & Macedonio, G. (2009). Fall3d: A computational model for transport and deposition of volcanic ash. *Computers & Geosciences*, 35(6), 1334–1342.
- Folch, A., Costa, A., & Macedonio, G. (2016). Fplume-1.0: An integral volcanic plume model accounting for ash aggregation. *Geoscientific Model Development*, 9(1), 431.
- Guo, S., Bluth, G. J., Rose, W. I., Watson, I. M., & Prata, A. (2004). Re-evaluation of so₂ release of the 15 june 1991 pinatubo eruption using ultraviolet and infrared satellite sensors. *Geochemistry, Geophysics, Geosystems*, 5(4).
- Guo, S., Rose, W. I., Bluth, G. J., & Watson, I. M. (2004). Particles in the great pinatubo volcanic cloud of june 1991: The role of ice. *Geochemistry, Geophysics, Geosystems*, 5(5).
- Holasek, R., Self, S., & Woods, A. (1996). Satellite observations and interpretation of the 1991 mount pinatubo eruption plumes. *Journal of Geophysical Research: Solid Earth*, 101(B12), 27635–27655.
- Holasek, R. E., Woods, A. W., & Self, S. (1996). Experiments on gas-ash separation processes in volcanic umbrella plumes. *Journal of volcanology and geothermal research*, 70(3-4), 169–181.
- Jäger, H. (1992). The pinatubo eruption cloud observed by lidar at garmisch-partenkirchen. *Geophysical research letters*, 19(2), 191–194.
- Mastin, L. G. (2007). A user-friendly one-dimensional model for wet volcanic plumes. *Geochemistry, Geophysics, Geosystems*, 8(3).
- Neri, A., Esposti Ongaro, T., Macedonio, G., & Gidaspow, D. (2003). Multiparticle simulation of collapsing volcanic columns and pyroclastic flow. *Journal of Geophysical Research: Solid Earth (1978–2012)*, 108(B4).
- Oberhuber, J. M., Herzog, M., Graf, H.-F., & Schwanke, K. (1998). Volcanic plume simulation on large scales. *Journal of Volcanology and Geothermal Research*, 87(1), 29–53.

- 663 Paladio-Melosantos, M. L. O., Solidum, R. U., Scott, W. E., Quiambao, R. B., Um-
 664 bal, J. V., Rodolfo, K. S., ... Ruelo, H. B. (1996). Tephra falls of the 1991
 665 eruptions of mount pinatubo. *Fire and mud*, 12000, 12030.
- 666 Pouget, S., Bursik, M., Singla, P., & Singh, T. (2016). Sensitivity analysis of a
 667 one-dimensional model of a volcanic plume with particle fallout and collapse
 668 behavior. *Journal of Volcanology and Geothermal Research*.
- 669 Schwaiger, H. F., Denlinger, R. P., & Mastin, L. G. (2012). Ash3d: A finite-volume,
 670 conservative numerical model for ash transport and tephra deposition. *Journal*
 671 *of Geophysical Research: Solid Earth*, 117(B4).
- 672 Scott, W. E., Hoblitt, R. P., Torres, R. C., Self, S., Martinez, M. M. L., & Nillos,
 673 T. (1996). Pyroclastic flows of the june 15, 1991, climactic eruption of mount
 674 pinatubo. *Fire and Mud: eruptions and lahars of Mount Pinatubo, Philippines*,
 675 545–570.
- 676 Searcy, C., Dean, K., & Stringer, W. (1998). Puff: A volcanic ash tracking and pre-
 677 diction model. *Journal of Volcanology and Geothermal Research*, 80, 1–16.
- 678 Self, S., Zhao, J.-X., Holasek, R. E., Torres, R. C., & King, A. J. (1996). The atmo-
 679 spheric impact of the 1991 mount pinatubo eruption.
- 680 Stefanescu, E., Patra, A., Bursik, M., Madankan, R., Pouget, S., Jones, M., ... oth-
 681 others (2014). Temporal, probabilistic mapping of ash clouds using wind field
 682 stochastic variability and uncertain eruption source parameters: Example of
 683 the 14 april 2010 eyjafjallajökull eruption. *Journal of Advances in Modeling*
 684 *Earth Systems*, 6(4), 1173–1184.
- 685 Suzuki, T., et al. (1983). A theoretical model for dispersion of tephra. *Arc volcan-
 686 ism: physics and tectonics*, 95, 113.
- 687 Suzuki, Y., & Koyaguchi, T. (2009). A three-dimensional numerical simulation
 688 of spreading umbrella clouds. *Journal of Geophysical Research: Solid Earth*
 689 (1978–2012), 114(B3).
- 690 Suzuki, Y. J., Koyaguchi, T., Ogawa, M., & Hachisu, I. (2005). A numerical study of
 691 turbulent mixing in eruption clouds using a three-dimensional fluid dynamics
 692 model. *Journal of Geophysical Research: Solid Earth*, 110(B8).
- 693 Tanaka, H. (1991). Development of a prediction scheme for the volcanic ash fall
 694 from redoubt volcano. In *First int'l. symp. on volcanic ash and aviation safety*
 695 (Vol. 58).
- 696 Walko, R., Tremback, C., & Bell, M. (1995). Hypact: The hybrid particle and con-
 697 centration transport model. *Users guide*.
- 698 Whitaker, J. S., Compo, G. P., Wei, X., & Hamill, T. M. (2004). Reanalysis with-
 699 out radiosondes using ensemble data assimilation. *Monthly Weather Review*,
 700 132(5), 1190–1200.
- 701 Witham, C., Hort, M., Potts, R., Servranckx, R., Husson, P., & Bonnardot, F.
 702 (2007). Comparison of vaac atmospheric dispersion models using the 1 novem-
 703 ber 2004 grimsvötn eruption. *Meteorological Applications*, 14(1), 27–38.
- 704 Woodhouse, M., Hogg, A., Phillips, J., & Sparks, R. (2013). Interaction between vol-
 705 canic plumes and wind during the 2010 eyjafjallajökull eruption, iceland. *Jour-*

706 *nal of Geophysical Research: Solid Earth*, 118(1), 92–109.

707 Woods, A. (1988). The fluid dynamics and thermodynamics of eruption columns.
 708 *Bulletin of Volcanology*, 50(3), 169–193.

709 Zidikheri, M. J., Lucas, C., & Potts, R. J. (2017). Estimation of optimal dispersion
 710 model source parameters using satellite detections of volcanic ash. *Journal of*
 711 *Geophysical Research: Atmospheres*, 122(15), 8207–8232.